



# 1 **Contrasting impact of different Mediterranean cyclones on the** 2 **hydrological cycle and ocean heat content**

3  
 4 **Yonatan Givon<sup>1</sup>, Douglas Keller Jr.<sup>2</sup>, Philippe Drobinski<sup>2</sup>, and Shira Raveh-Rubin<sup>1</sup>**

5  
 6 <sup>1</sup> Department of Earth and Planetary Sciences, Weizmann Institute of Science, Rehovot, Israel

7 <sup>2</sup> Laboratoire de Météorologie Dynamique-IPSL, École Polytechnique, Institut Polytechnique de Paris, ENS,  
 8 PSL Research University, Sorbonne Université, CNRS, Palaiseau, France  
 9

10 *Correspondence to: Yonatan Givon ([Yonatan.givon@weizmann.ac.il](mailto:Yonatan.givon@weizmann.ac.il))*

11  
 12 **Abstract.** Mediterranean cyclones (MCs) play a crucial role in the Mediterranean hydrological cycle (MHC),  
 13 driving up to 70% of precipitation and 50% of evaporation totals, and larger fractions of their extremes. Therefore,  
 14 regional sensitivity to warming is often associated with long-term changes of MCs. These may lead to regional  
 15 climate feedback through pathways linked directly or indirectly to the MHC: from decreasing cloud cover and  
 16 precipitation to increased water-vapor uptake. However, the ability of MCs to generate coherent climate feedback  
 17 is under ongoing debate. Moreover, given the large diversity of processes driving MCs, the role of each in the  
 18 MHC and their variability remains unexplored. Our recent process-based MC classification allows the breakdown  
 19 of MC's contribution to the MHC under different dominant cyclogenetic processes. Based on 1-hourly ECMWF  
 20 ERA5 reanalysis data (1979-2020), 3190 MC tracks are analyzed. We first quantify the total contribution of MCs  
 21 to the MHC following the cyclone tracks. We analyze the spatial and temporal patterns of the annually  
 22 accumulated cyclone-induced precipitation (P) and surface evaporation (E). The process-based classification  
 23 allows the quantification of independent contributions from various cyclone drivers to cyclone-induced P and E  
 24 and their long-term trends. The results show that the overall annual P-E residual associated with MCs is positive  
 25 but decreases over time, losing ~0.5 mm/yr per year. The classification reveals opposing roles and long-term  
 26 trends in the annual contributions of each cyclone driver, shifting the balance between cyclone-induced P and E  
 27 from P-dominated towards E-dominated MCs. These changes are primarily due to reduced precipitation associated  
 28 with double-jet MCs and daughter cyclones and increased evaporation associated with thermal lows (-0.2  
 29 mm/year, each), alternately driven by changes in frequency and/or flux intensities of specific cyclone drivers.  
 30 Mainly, a sharp rise in frequency affects heat lows, while double-jet cyclones are mostly affected by decreasing  
 31 precipitation rates. The downward impact of MCs on the Mediterranean Sea heat content also varies sharply  
 32 between MC types: while MCs generally draw heat from the Mediterranean, certain MC types have the opposing  
 33 effect, adding further heat. Beyond providing a framework for follow-up analysis of MC impact on the MHC in  
 34 future climate simulations, the results highlight the independent and opposing contributions of different MC  
 35 drivers to the Mediterranean heat content, enhancing our understanding of their dynamic response to warming and  
 36 its impact on society.

37



## 1. Introduction:

Extratropical cyclones are prominent low pressure weather systems that strongly influence the hydrological cycle, as they drive heavy precipitation (P) and evaporation (E). While the link between cyclones and P is well defined through their forced uplifting, E involves more complex relationships with cyclone-induced perturbations via wind speed, humidity and temperature.

The Mediterranean Sea hosts a unique subset of cyclones in the transition zone between the sub- and extra-tropics. Mediterranean cyclones (MCs) differ from other open-ocean cyclones primarily in their compact spatial structure and the diverse influences of orography, strong land-sea contrast, and relatively warm sea surface temperatures (Flaounas et al., 2022). As a result, MCs are considered challenging to predict and represent in models on both weather and climate scales (Lionello et al., 2007; Hatzaki et al., 2023), with their transient manifestation as extra-tropical cyclones, subtropical heat lows, and rare tropical-like cyclones (Flaounas et al., 2015).

Beyond their socio-economic impacts, reviewed recently by Khodayar et al., (2025), MCs have a significant influence on the Mediterranean hydrological cycle (MHC), driving extreme E and P rates and accounting for considerable portions of the overall air-sea exchange of freshwater fluxes (Lebeauin Brossier et al., 2014; Flaounas et al., 2016). Due to their dominance on the MHC, long-term variations in features of MCs are often used to explain the regional sensitivity to climate change (Lionello et al., 2007; Hochman et al., 2020; Reale et al., 2022; Zittis et al., 2022). Specifically, regions prone to moistening are expected to get more of it, and vice versa for regions prone to drying. This phenomenon is often referred to as the “wet gets wetter - dry gets drier” mechanism, often explained by a rise in MC-associated P due to increased water-vapor uptake caused by the rise in temperatures, and a drying effect as MCs grow less frequent in the southern and eastern Mediterranean due to the meridional shift of the Atlantic storm track (Chericoni et al., 2025).

However, the direct link to cyclone properties is usually implied rather than shown, and it remains unclear how MCs respond to and affect the regional climate changes through their contribution to P (Zappa et al., 2015; Zittis et al., 2019; Scoccimarro et al., 2025) and E (Flaounas et al., 2019; Reale et al., 2021). While in the tropics enhanced E rates are deemed necessary to sustain cyclones and generate P, in the extra-tropics, extreme evaporation rates may arise preferentially in their cold sector. In the cold sector, under the wake of cyclone and frontal passage, E typically peaks under cold air outbreaks (Papritz et al., 2015; Thurnherr et al., 2020) and dry intrusions, namely, large-scale descending air streams of extratropical cyclones, that amplify surface evaporation through the penetration of dry air masses with strong wind speeds from upper levels to the surface boundary layer (Raveh-Rubin 2017; Ilotoviz et al., 2021; Rai and Raveh Rubin 2023; Klaider and Raveh-Rubin 2023; Givon et al., 2024b). While the frequency of extratropical-like MCs (most comparable to extratropical cyclones) is expected to decrease (Nissen et al., 2014), uncertainty exists regarding their projected intensification under global warming, changing their overall contribution to the MHC and being inconsistent among climate models (Gaertner et al., 2007). Lionello et al., (2007) investigated projected changes in cyclone activity over Europe, including the Mediterranean basin, and emphasized the importance of regional characterization of changes in cyclonic activity, due to the large variability among MCs.

Changes in water availability are often measured using the difference between E and P, with recent work (Tootoonchi et al., 2025) indicating MCs (transient eddies) as the major driver of humidity convergence from the



ocean sources to adjacent land sinks, pointing out their importance for the atmospheric branch of the MHC. Flaounas et al., (2016) used an intensity-dependent cyclone impact area to analyze the climatological contribution of MCs to the atmospheric MHC in coupled, high-resolution WRF (atmosphere) and NEMO (ocean) simulations. Their results show up to 90% of P extremes (95<sup>th</sup> percentile) and up to 70% of extreme E rates associated with MCs. The study further evaluates the annual contribution of MCs to the MHC, suggesting a small residual (E-P). They conclude that MCs sustain a balance between their induced E and P on longer time scales, suggesting that changes in their contributions are unlikely to substantially alter the future MHC.

Nevertheless, considering the various manifestations of MCs, it is important to know whether their role in the MHC differs by driving mechanism, as each may pose a different direction of response to climate change. Givon et al., (2024a) revealed the potential of classifying MC tracks by their dominant large-scale driver to enhance the dynamical understanding of MCs and their long-term variability. This classification was adopted by Rousseau-Rizzi et al., (2024), Portal et al., (2024), and Portal et al., (2025) to analyze MC-related compound hazards and extremes (including P) and investigate their convective features. By separating MC tracks into 9 distinct groups indicative of different dominant cyclogenetic processes, the fundamentally different life cycles and weather impacts of each MC driver were revealed, allowing the decomposition of the hydrological contribution of MCs into a spectrum of MC drivers.

Primarily through their intense evaporation rates, MCs (and cyclones in general) are effective at extracting latent and sensible heat from the ocean. While several studies have focused on the cooling effect of regional gap-wind regimes such as the mistral and bora winds (Berthou et al., 2018; Flamant 2003) on sea surface temperatures, literature focusing on the direct impact of MCs on the ocean heat content (OHC) is scarce. Givon et al., (2024b), for example, systematically analyzed ocean evaporation fluxes associated with the mistral, emphasizing the role of downward advection of upper-level momentum by dry intrusions in the generation of extreme evaporation rates. Keller et al., (2022) and (2024) and Keller (2025) further consolidated the importance of the mistral wind to deep water formation in the Gulf of Lion. However, how different MC drivers impact the Mediterranean OHC is not well known. Since OHC is often considered as an energy source for developing MCs (Stathopoulos et al., 2020; Strobach et al., 2024), especially tropical-like ones (“Medicanes”, Cavicchia et al., 2014; Jangir et al., 2024), we aim to evaluate which MC types are the most influential for the OHC in different regions across the Mediterranean basin. It is important to reveal subtle changes in the ability of MCs to extract heat from the ocean, as they may impair the climatological role of MCs as cooling agents in the oceanic system. Analyzing the impact of the various MC drivers on both the MHC and OHC will allow a better understanding of future changes in the Mediterranean climate. Therefore, our research objectives are threefold:

1. Quantify overall cyclone contribution to the mean annual MHC (P, E and P-E), and decompose this to different MC drivers (following Givon et al., 2024a)
2. Reveal historical trends in (1)
3. Evaluate the influence of (1) on the OHC

For this study, we use comprehensive cyclone track data, generated through a composite cyclone detection algorithm (Flaounas et al., 2023) based on ECMWF ERA5 reanalysis (1979-2020) and apply the cyclone-centered potential vorticity (PV) classification presented by Givon et al., (2024a). We define a cyclone impact area to



114 accumulate surface evaporation and precipitation throughout each cyclone track and obtain the cyclone-induced  
 115 fluxes. We then separate each MC track into the 9 classes and evaluate the long-term trends in the annually  
 116 accumulated precipitation and evaporation. Finally, we use a NEMO simulation forced by ERA5 to quantify the  
 117 impact of MCs on the OHC, examining the cyclone-induced heat loss of the Mediterranean.

## 118 **2. Methods:**

### 119 **2.1. Cyclone detection and tracking**

120 MCs are here detected and tracked based on a composite cyclone detection algorithm presented by Flaounas et  
 121 al., (2023) and used by Givon et al., (2024a) for the dynamic classification of MCs. With this approach, 10  
 122 different tracking methods are applied to 1-hourly ERA5 reanalysis of ECMWF (Hersbach et al., 2020).  
 123 Confidence level 5 is chosen, denoting the agreement of at least 5 detection methods on every MC track. Each  
 124 composite cyclone track contains the location of its center throughout its lifetime. Sea level pressure at the cyclone  
 125 center is also reported, and its minimum along the track is used to define MC peak time for classification. Some  
 126 cyclone tracks that do not cross east of longitude 5°E are removed from the analysis, see more details in Givon et  
 127 al., (2024a). Overall, 3190 MC tracks are captured throughout the period, with a minimum lifetime of two days.

### 128 **2.2. Process-based classification**

129 Here, we utilize the cluster separation presented in Givon et al., (2024a). Specifically, for each MC at peak  
 130 intensity, the surrounding upper-level isentropic potential vorticity field (PV, vertically averaged between the 320-  
 131 340K isentropic levels) is extracted around the cyclone center. The PV field is considered within a domain  
 132 extending 20° east and west of the MC center, 40° to the north and 20° to the south. The PV field is classified using  
 133 a self-organizing map algorithm (SOM), producing 9 robust clusters with distinct Rossby wave patterns, unique  
 134 surface impacts, and inherent characteristics. Here, we attribute the cluster number originally determined for the  
 135 cyclone peak time throughout the cyclone's lifetime.

### 136 **2.3. MC impact area**

137 We integrate the hourly P and E accumulated along each MC track to derive MC-induced freshwater fluxes. To  
 138 attribute the fluxes to the MC track and allow an objective comparison of the different MC types we define a  
 139 constant 10° radius impact area around the cyclone center, within which the fluxes are accumulated in 1-hourly  
 140 steps along the track. This ensures that no cluster is favored or penalized by impact area differences. While a 10°  
 141 radius may be considered excessive to associate to MCs (Flaounas et al., 2016), it has been adopted by recent  
 142 studies on MC impacts (Rousseau-Rizzi et al., 2024 and Portal et al., 2024). Results show little sensitivity to the  
 143 MC impact area in the present framework: with a 5° radius, the spatially accumulated cyclone-induced fluxes  
 144 naturally decrease, but the fundamental differences among the MC types and their temporal variability are  
 145 unchanged. Area-weighted averages are calculated across the MC impact area and accumulated annually to  
 146 quantify total MC-induced fluxes.

147 To investigate interannual trends in MC-induced evaporation and precipitation, we accumulate freshwater fluxes  
 148 spatially and temporally across each year, integrating along the MC tracks. We thus obtain a Lagrangian  
 149 framework used to unveil the cyclone-driven component of the MHC under a process-based prism, resulting in a  
 150 novel hydrological-budget analysis of differently driven MCs.



151

#### 152 **2.4. Normalization by MC frequency**

153 As noted by Zappa (2014), changes in MC-induced P are influenced by both changes in MC frequency and  
 154 intensity. A similar argument can be made for MC-induced E. To address both sources of variance, we complement  
 155 the accumulated MHC contributions with their normalized ones. To eliminate variations in frequency and obtain  
 156 the fluxes per cyclone, normalized P and E are evaluated as follows:

$$157 \quad P_{norm} = \bar{F}_{MC} \sum_y \frac{P_y}{F_y}$$

$$158 \quad E_{norm} = \bar{F}_{MC} \sum_y \frac{E_y}{F_y}$$

159 Where  $P_y, E_y$  stands for annual cyclone-induced precipitation and evaporation, respectively,  $F_y$  denotes the  
 160 corresponding annual frequency of MCs, and  $\bar{F}_{MC}$  denotes the mean MC frequency across all years. The frequency  
 161 accounts for the co-occurrence of multiple cyclones in the domain by counting the number of MC centers at every  
 162 time step. Although this approach leads to large annual frequencies (up to 80%, as also recognized by Flaounas et  
 163 al., 2016), it ensures the overall conservation of mass. We similarly normalize the contributions from each cluster  
 164 to reveal MC types that are more susceptible to these elusive changes in intensity.

#### 165 **2.5. Ocean heat content**

166 Ocean heat content (OHC) in the layer 0-300 m is computed using the Euro-Mediterranean Center on Climate  
 167 Change (CMCC-Foundation) eddy-permitting global ocean reanalysis, C-GLORS v7. The model data is provided  
 168 at daily frequency from 1993 up to 2019 and 1/4° horizontal resolution with 50 vertical levels. Details on the  
 169 model and improvements from previous versions are presented by Storto and Masina (2016). While suffering  
 170 from low temporal resolution and a shorter temporal extent, the model proves valuable for process-based research  
 171 on heat exchanges, in agreement with comparable independent estimates.

172 To investigate the impact of the various MC drivers on the OHC, we use a 6-day window centered at the location  
 173 of each MC at peak intensity times and map the net difference in OHC before and after an MC passage. These  
 174 differences are accumulated under the impact area at MC peak time on daily resolution and separated by cluster.  
 175 The OHC is a measure of stored energy. As such, temporal changes in it can be interpreted as energy fluxes and  
 176 are indeed affected by atmospheric fluxes of both sensible and latent heat. However, the OHC is affected by other  
 177 processes as well, such as radiative and advective fluxes. Nevertheless, since the presence of MCs potentially  
 178 influences all of these, and with the presence of cyclones being the only common feature of the observed data, the  
 179 OHC response is interpreted as MC-driven fluxes for consistency. We thus convert the OHC difference (originally  
 180 measured in Joules) to units of virtual evaporation rates ( $E_v$ , mm/year) as follows:

$$181 \quad E_v = (365 * \bar{F}_{MC_d}) \frac{(OHC_{t_0+3} - OHC_{t_0-3})}{6 \text{ days}} L_v$$



182 Where  $\bar{F}_{MC_d}$  stands for the annual-mean frequency of MCs on daily scale (either as a whole or per cluster)  
 183 considering only the peak-time ( $t_0$ ) of each track, and  $L_v$  is the latent heat of evaporation. This way, the MC impact  
 184 on the OHC is comparable to the atmospheric freshwater fluxes.

185 We note that this analysis does not fully disentangle the impact of the OHC on MCs, that tend to intensify with  
 186 response to large OHC values. Nevertheless, the temporal evolution of the difference in OHC (not shown) suggests  
 187 that the OHC response is temporally centered around the passage of MCs and provides a direct measure of the  
 188 MC-related ocean-heat loss. We interpret the results as the impact of MCs on OHC, while admitting that MC  
 189 intensity is partially impacted by initially high OHC values. The agreement between the MC-driven E and OHC  
 190 response to MC supports this interpretation. In the future, we aim to further address this two-way coupling between  
 191 MCs and the OHC in a dedicated study.

### 192 **3. Results**

#### 193 **3.1. MCs overall contribution to the MHC**

194 We begin with a climatological overview of the MHC (Fig. 1 panels a and b), followed by the MC contribution to  
 195 mean annual P and E. Overall, P is shown to mainly affect coastal areas and mountain ridges, reaching values up  
 196 to 1500 mm/year, whereas E dominates over the maritime regions and is minimal over land. In agreement with  
 197 previous studies (Flaounas et al., 2016; Tootoonchi et al., 2025), the results highlight the prominence of MCs on  
 198 the MHC, driving up to 70% of total precipitation and up to 50% of total surface evaporation in various regions  
 199 (Fig. 1 panels c and d). While the contribution of MCs to E overlaps well with cyclone density, the peaks of MC  
 200 contribution to P are shifted eastwards. This is in line with the findings of Saaroni et al., (2010), highlighting the  
 201 strong dependance of eastern Mediterranean rainfall on MCs. We note that the contribution of MCs to total surface  
 202 evaporation is about twice their mean frequency, while their contribution to precipitation is about three times  
 203 higher, indicating that MC-induced freshwater fluxes are strongly concentrated within the MC impact area rather  
 204 than resulting from random spatial overlaps.

205 When examining the area-weighted accumulated fluxes in Fig. 2, grid points affected by MCs show higher P and  
 206 E mean rates compared to the year-round average regardless of MC presence in the domain (compare panels a  
 207 and b). While both P and E of MCs (Fig. 2b) are slightly increasing with time, the positive residual (P-E) associated  
 208 with MCs is being gradually eroded. The normalized fluxes (Fig. 2c) reveal a decrease in P and an increase in E  
 209 per cyclone. Interestingly, the covariance between MC-induced P and E is solely due to their shared MC  
 210 frequencies, dropping to zero for the normalized E and P (Fig. 2c). This result suggests that instantaneous E and  
 211 P rates are unconstrained when observed per cyclone, as MCs converge moisture from other sources in addition  
 212 to their self-induced E to generate heavy P rates. To better understand the sources of these long-term variabilities,  
 213 we examine the results under the nine dominant MC drivers.

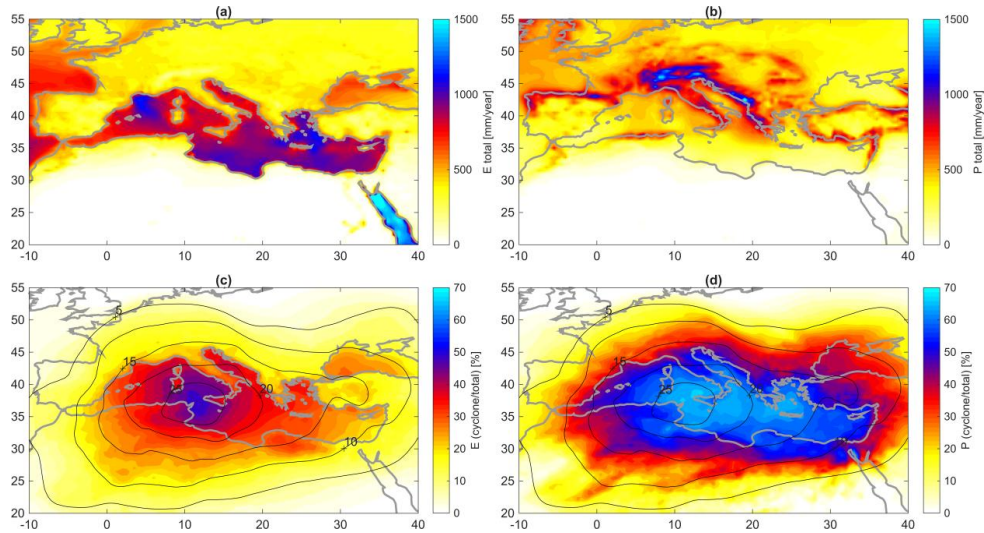


Figure 1: Annual-mean  $E$  (a) and  $P$  (b), and the relative contribution of MCs to both (c and d, shading,  $E$  and  $P$  respectively) along with mean cyclone frequency  $\bar{F}_{MC}$  (black contours, %).

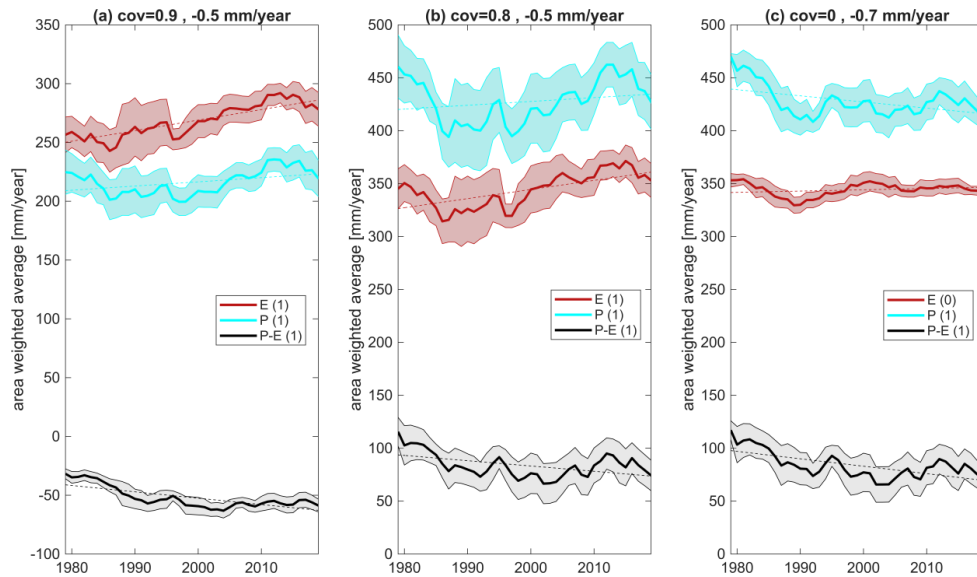


Figure 2: (a) 8-year moving mean ( $\pm 1$  STD, shading) of total  $E$  (red),  $P$  (cyan), and  $P-E$  (black) within the domain shown in Figure 1 (10E–40W, 20N–55N). Dashed lines denote the corresponding linear best-fit. The result of a 95% confidence level Mann-Kendall test for each component is shown in the legend (1 for a significant trend). (b) as in (a), but for the cyclone-induced  $E$  and  $P$ , considering only the cyclone impact area. (c)  $P_{norm}$ ,  $E_{norm}$ , i.e., as in (b) but normalized by annual cyclone frequency (hourly, including double counts), representing flux intensities. Titles denote the covariance factor between  $P$  and  $E$  followed by the slope of the linear best-fit (mm/year) for the  $P-E$  trends.





### 225            **3.2. MC contribution to the MHC by cluster**

226        Under the cyclone-centered PV classification, the complexity and competing effects of the various MC drivers on  
227        the MHC is clarified. Fig. 3 highlights the variability between the different MC drivers at peak cyclone intensity.  
228        Cluster 4, representing fully developed baroclinic MCs, shows the most intense instantaneous E and P fluxes while  
229        cluster 6, typically impacting North Africa, is associated with much weaker freshwater exchanges. However, sharp  
230        differences are also evident between clusters that share similar seasonal and geographical amplitudes, such as  
231        clusters 1, 2, and 4, and clusters 3, 5, and 7. Cluster 8, associated with narrow, cyclonically curving PV streamers,  
232        and recently found to be the most favorable for deep convection (Portal et al., 2025), notably exhibits the most  
233        intense fluxes among the off-winter clusters.

234        We note that the impact area well captures the E and P features associated with MCs. The relatively strong  
235        evaporation observed about 15° to the west of the MC centers of clusters 3, 5, and 7 (i.e., outside of the impact  
236        area) mostly occurs over the Atlantic Ocean, given their preferred locations (see Fig. 7 in Givon et al., 2024a).  
237        With this MC-centered view it appears that a first-order correlation exists between instantaneous MC induced E  
238        and P. However, since some of the clusters appear more frequently on land, we next evaluate the accumulated  
239        fluxes throughout the MC duration and consider their geographical areas of influence.



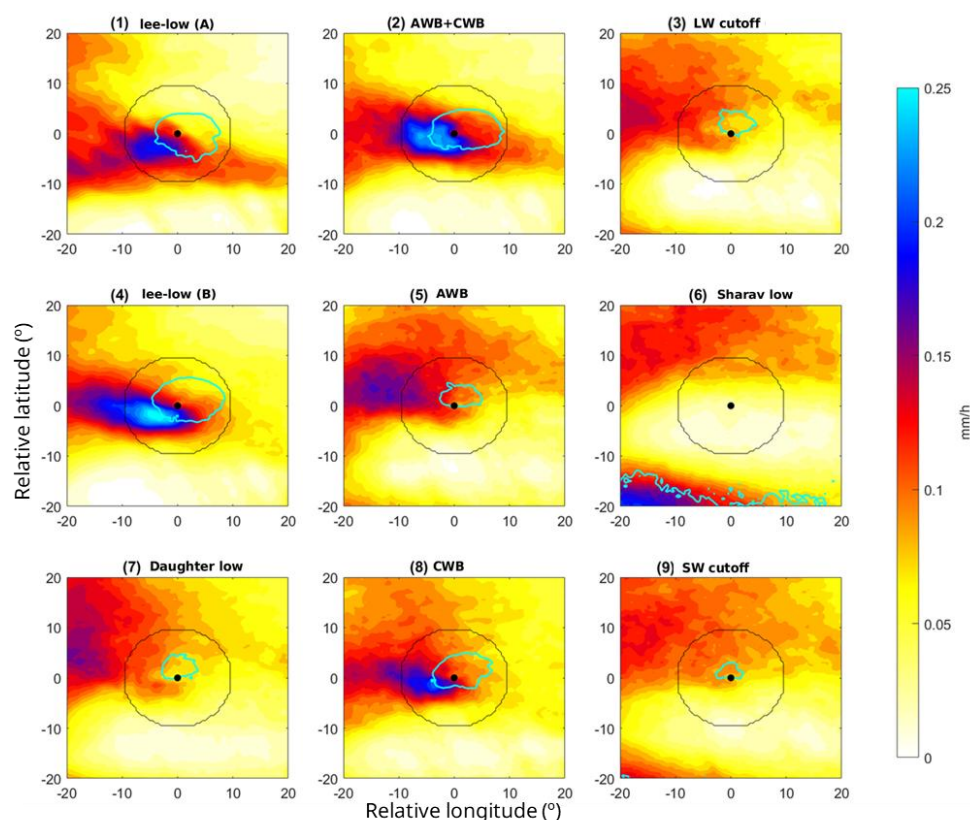
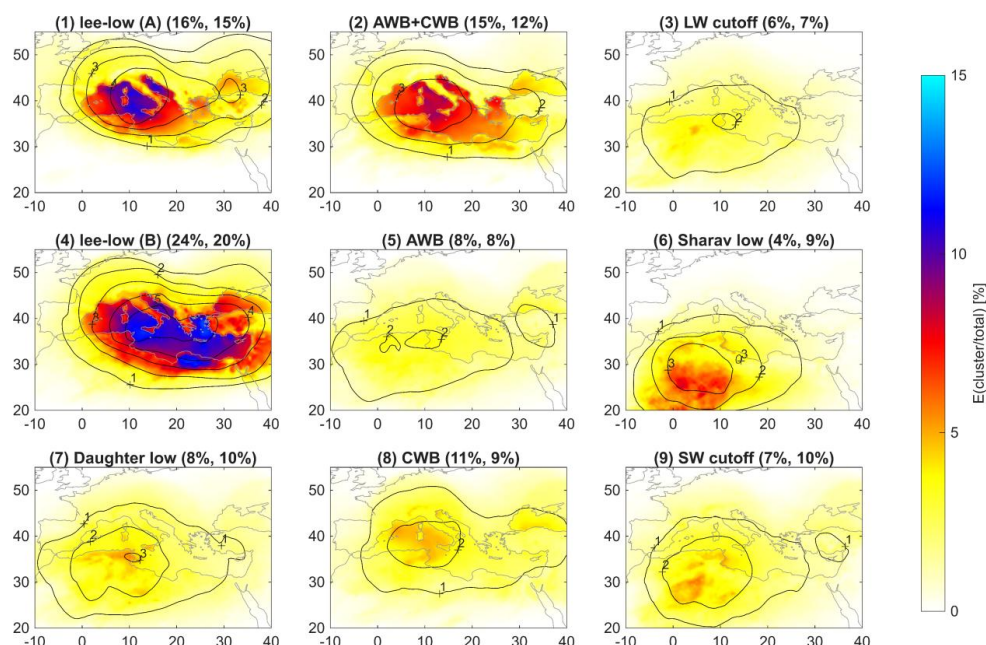


Figure 3: cyclone-centered cluster composites of  $E$  (shading) and  $P$  (cyan contours, 0.25 mm/h) at classification time (minimum SLP time of each MC track). The black circles denote the  $10^\circ$  radius impact area considered for cyclone-induced fluxes.

The independent contributions of each MC type to the overall annual  $E$  are shown in Fig. 4. Cluster 4 stands out as a major contributor, accounting for up to 24% of the MC-induced  $E$  despite forming 20% of the total MC frequency (see Fig. 4 titles). The ratio between the MC contribution and local frequency surpasses 3 in the eastern Mediterranean and along the north African coast, suggesting high conditional probability. Cluster 1, representing cold cyclones anchored to topography, shows significant  $E$  contributions especially in the Ligurian and Adriatic seas, as may be expected from the strong gap-winds regimes triggered at the early stages of Alpine lee-cyclogenesis and their link to evaporation (Buzzi et al., 2020, Givon et al., 2021, Givon et al., 2024b). On the other hand, the contributions of summer clusters 6 and 9 are weaker than their mean frequency, which is often over land, possibly due to already high evaporation rates throughout the season (Ruiz et al., 2008). Nevertheless, Sharav lows (North-African heat lows captured by cluster 6) are associated with strong evaporation hot-spots in north-western Africa, possibly affecting the great lakes and land-moisture in the region (Rieder et al., 2025). The double-jet configuration denoted by cluster 2 notably contributes 15% to total MC-induced evaporation despite its 12% relative frequency, suggesting strong – yet apparently more local – evaporative capabilities, appearing as relatively sporadic evaporation hotspots.

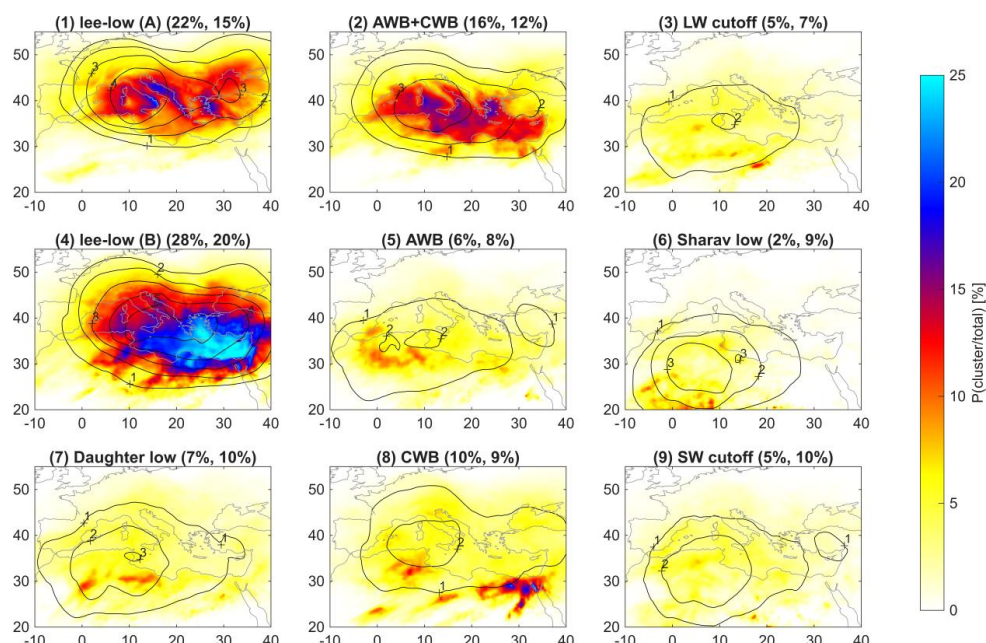


258

259 *Figure 4: Relative contribution of each cluster to total E (shading, %) and cluster mask frequency (black contours,*  
 260 *%, in 1% intervals). Titles denote cluster numbers and the dominant driving mechanism as reported in Givon et*  
 261 *al., (2024a). Numbers in brackets indicate the mean contribution of each cluster to total MC-induced surface*  
 262 *evaporation (left) and the mean cluster frequency out of all MCs (right).*

263 The cluster-separation of contributions to P is even more pronounced (Fig. 5). Cluster 4 dominates in the central  
 264 and eastern Mediterranean, overall contributing 28% of total MC induced P, and cluster 1 in the western coasts of  
 265 Italy, Greece and Turkey, and along the Adriatic, providing 22% of total MC induced P. The precipitation induced  
 266 by cluster 2 again exhibits some local effects, while the contributions of the other clusters are significantly weaker.  
 267 Intriguingly, precipitation along the Egyptian coast shows a tight link to cyclonic wave breaking (CWB) MCs  
 268 captured in cluster 8, with ~20% of annual precipitation delivered in a mere 1% regional cluster frequency.  
 269 Moreover, this region is hardly responsive to other MC clusters.

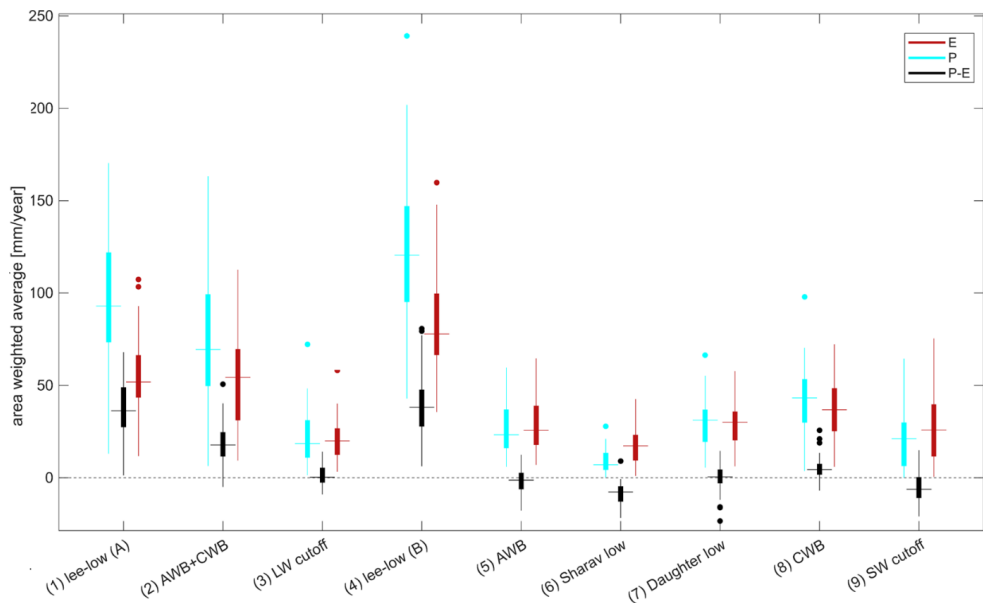
270 These results illustrate well the robustness of the PV clustering even beyond the classification time, with profound  
 271 implications on geographical, seasonal, and dynamical variability. Each MC driver thus plays a fundamentally  
 272 different role in shaping the MHC.



273

274 *Figure 5: As Figure 4 but for P.*

275 To evaluate the total contribution of MCs and their drivers to the MHC, we accumulate the fluxes spatially and  
 276 temporally across the years, analyzing both annual P and E distributions as well as their difference, P-E, per  
 277 cluster. Fig. 6 shows that the overall slightly positive P-E contribution of MCs is the result of a delicate balance  
 278 between inherently imbalanced MC contributions: while winter clusters 1, 2, and 4 act as moisture sources, each  
 279 adding about 30 mm/year per grid-point within a 10° radius impact area, these inputs are partly offset by a  
 280 consistent drying effect imposed by the summer-prone clusters 5, 6, and 9. Seeing as the relative frequencies of  
 281 each cluster are changing in recent decades (Givon et al., 2024a), we further analyze the long-term variability of  
 282 each cluster, accounting for both variations in frequency and intensity.



283  
284 *Figure 6: Distributions of area weighted annual mean MC-induced E, P, and P-E, separated by cluster. The*  
285 *medians of each distribution are denoted by the horizontal lines, the boxes mark the 25 to 75 percentiles of the*  
286 *distribution, and whiskers mark the 2.5 and 97.5 percentiles, setting the threshold for outliers, marked by the*  
287 *colored dots.*

288 **3.3. Long-term variability by cluster**

289 Long term variability of MC occurrence and interaction with the MHC strongly depends also on MC cluster type.  
290 The relative importance of each MC cluster is shifting over recent decades, as shown in Fig. 7. While some clusters  
291 are well balanced and hardly contribute to the MC-induced P-E (e.g., clusters 5 and 9), P-E is growing larger for  
292 some (clusters 1, 3, and 8) and smaller for others (clusters 2, 4, 6, and 7). The strongest change is captured for the  
293 double-jet cluster 2, losing 0.2 mm/year which corresponds to ~1% erosion of its annual precipitation surplus per  
294 year, with similar trend magnitudes reported for clusters 6 and 7. The net negative contributions from clusters 2,  
295 4, 6, and 7 differentially stem from either a reduction in precipitation (clusters 4 and 7), an increase in evaporation  
296 (6), or both (cluster 2). By contrast, cluster 8 contribution is positive and slightly increasing with time, due to  
297 enhanced P and near-constant E. As these changes can arise from either changes in frequency or intensity, we next  
298 examine the normalized fluxes and their trends, effectively eliminating frequency changes and highlighting  
299 changes in E and P intensities.

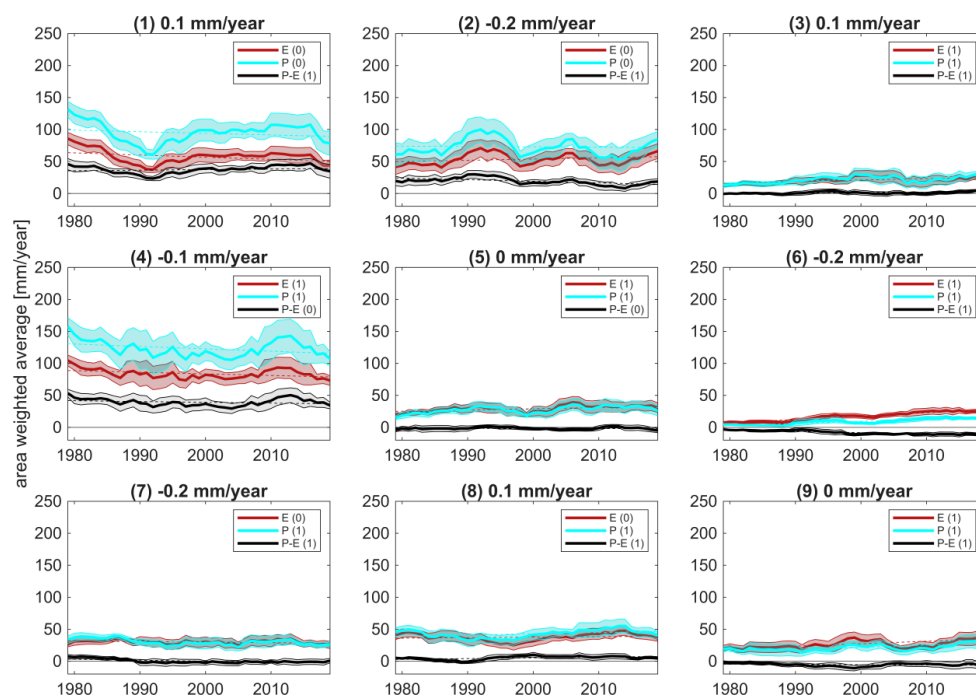
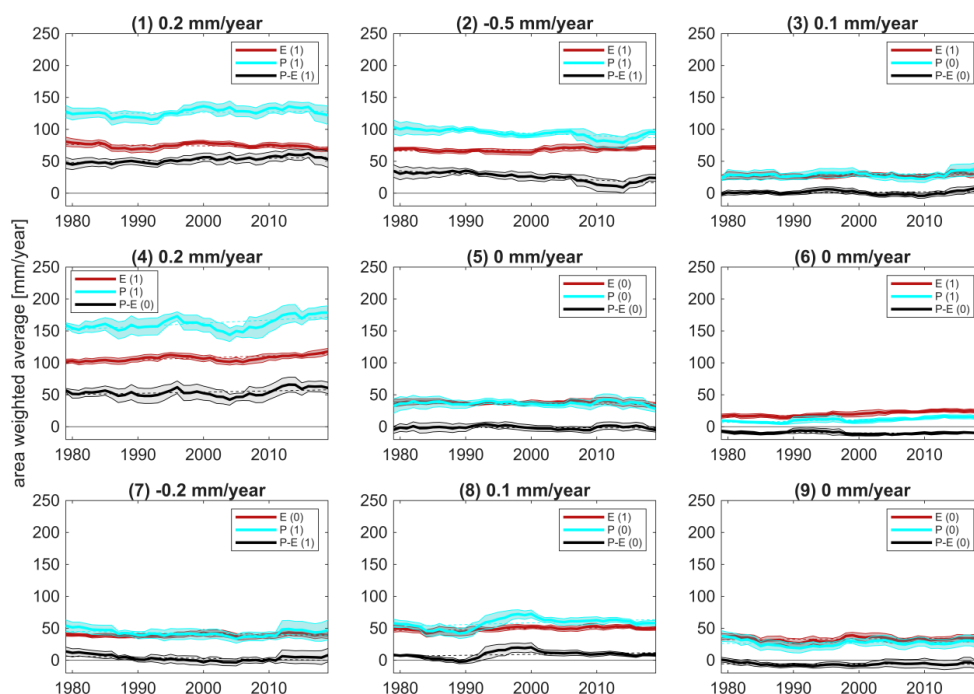


Figure 7: As Figure 2 (b) but separated by cluster. Titles denote the cluster number followed by the slope of the linear best-fit (mm/year) for the P-E trend. The result of a 95% confidence level Mann-Kendall test for each component is shown in the legend (1 for a significant trend)

Indeed, the net contributions (P-E) of each cluster vary differently when only changes of flux intensity are considered (Fig. 8). The intensity-only loss from cluster 2 is enhanced to -0.5 mm/year, indicating that its increasing frequency masks a drop in intensity. Interestingly, the  $E_{\text{norm}}$  and  $P_{\text{norm}}$  associated with cluster 2 evolve in opposite directions, with decreasing  $P_{\text{norm}}$  (and increasing  $E_{\text{norm}}$ ). As suggested by previous studies, the overall drop in precipitation for cluster 4 is indeed driven solely by a reduction in frequency, while the intensity of both  $E_{\text{norm}}$  and  $P_{\text{norm}}$  steadily increase. For cluster 6, changes in intensity exist but are well balanced, suggesting changes in frequency are dominant in determining P-E for these Saharan heat lows.

When separated by cluster, the P-E residual shows distinct long-term trends that are affected by variations in both frequency and intensity. In agreement with previous studies, winter MCs grow in intensity and decrease in frequency, with the latter being more dominant, resulting in a long-term reduction in P-E. Summer MCs, on the other hand, are primarily affected by a rise in frequency, leading to further drying.





315

316 *Figure 8: As Figure 7 but normalized by cluster frequencies, highlighting flux-intensity variations.*

317 To derive the overall impact of MCs on the MHC, net cluster frequencies and their area weighted  
 318 contributions to the MHC relative to accumulated climatological values across space and time are  
 319 shown in Table 1. The net frequencies consider the temporal occurrence of each MC cluster and the  
 320 ratio between the number of grid-points within the MC masks to the total number of grid points in the  
 321 domain. These frequencies hence describe the fraction of MC affected areas throughout the entire  
 322 analysis period and across the whole domain. The overall net climatological P-E in the Mediterranean  
 323 is -52 mm/y (Fig. 2a). The overall MC-induced P-E is, however, positive, counter balancing 24% of the  
 324 climatological negative P-E. The MC contribution is primarily driven by lee-cyclones (clusters 1 and  
 325 4), while specific MC drivers (clusters 5, 6 and 9) act to enhance the overall excess E in the  
 326 Mediterranean.



Cluster	Net Freq. (%)	E (%)	P (%)	P-E (%)
1	2.0	2.6	5.1	10.7
2	1.6	2.5	4.0	5.5
3	0.9	0.9	1.2	0.6
4	2.6	3.9	6.6	10.4
5	1.1	1.2	1.4	-0.2
6	1.2	0.7	0.5	-2.2
7	1.3	1.3	1.6	0.3
8	1.3	1.7	2.2	1.4
9	1.3	1.2	1.1	-1.4
All	13.4	15.5	22.9	24.1

Table 1: total cluster spatio-temporal frequencies and corresponding MHC contributions relative to the total accumulation of the climatological values across the domain. 'All' stands for all MC clusters combined.

### 3.4. MC-induced OHC perturbations

The overall impact of MCs on the OHC (Fig. 9) shows that on average, MCs extract heat from the Mediterranean at a mean rate equivalent to 645 mm/year of E. Although other processes affect the OHC, including lateral advection and radiative effects, the contribution of MC induced E alone accounts for up to ~350 mm/year (Fig. 2), more than 50% of the net OHC difference with response to the passage of MCs. Notably, the OHC response to MCs is positive along the North-African and eastern Mediterranean coasts, suggesting MCs tend to add heat to these areas. While this local reversal could be the result of sensible heat fluxes triggered by heat lows that often affect these areas, further research into oceanic flows is required to definitively explain these signals.

Once more, the cluster breakdown provides a more detailed picture of the independent role of MC types (Fig. 10): MC drivers that provide excess P also appear to drain heat from the ocean (clusters 1, 2, 4, and 8), as their E is still higher than that of E-dominated MCs. The E-dominated MCs (clusters 6, 7, and 9) act as heat sources, enhancing the OHC as they evolve rather than lowering it. This may be the result of their dry formation environments, prohibiting precipitation and leading to convergence of dry, warm air towards the MC center, generating enhanced downward sensible and possibly radiative (i.e., reduced cloud cover) fluxes. Spatial variability is evident for some of the clusters, suggesting certain drivers, e.g. clusters 3 and 5, act differently in different regions. Specifically, these MCs act as heat extractors when impacting the eastern Mediterranean, and heat suppliers when impacting the western parts. The OHC response to the various MC drivers is in-line with the atmospheric perspective, suggesting that opposing contributions of MCs to the MHC also bear the opposite impact on the MHC. This highlights the importance of considering the internal variability of MCs when assessing their role in future climate.



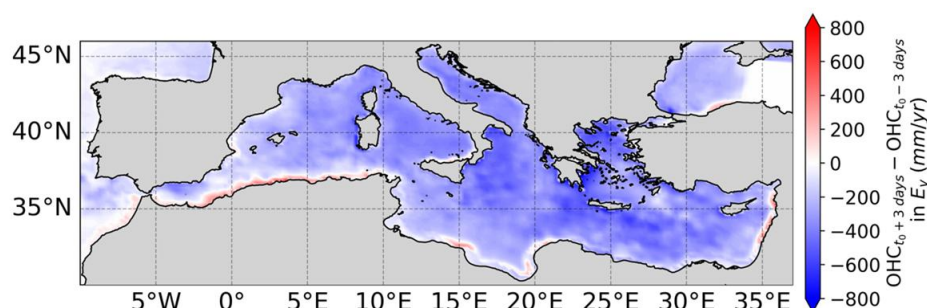


Figure 9: Composites of the difference in ocean heat content  $\pm 3$  days before and after the influence of a MC, normalized by annual MC frequencies. Negative values indicate net heat extracted from the ocean towards the atmosphere.

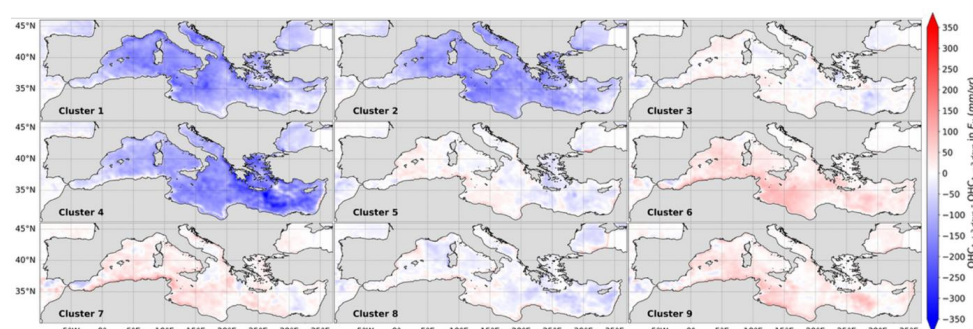


Figure 10: As Figure 9 but separated into clusters. Note that the values are normalized by annual MC cluster frequencies, thus representing the net heat taken from (negative values) and added to (positive values) the Mediterranean per cluster, per year.

#### 4. Discussion

This work investigates the impact of MCs on precipitation (P), evaporation (E), and the P-E residual as well as Mediterranean ocean heat content (OHC), separating between the independent contributions of 9 dominant MC drivers. MCs account for up to 70% of annual P and 50% of annual E, but the contribution to each component is highly asymmetric when separated by MC driver, as captured by the cyclone-centered PV-based clusters (Givon et al., 2024a). Cluster-dependent trends in cyclone-induced P, E, and P-E are revealed, controlled both by changes in MC cluster frequencies and in instantaneous flux intensities. The net annual P-E of MCs is positive and slightly decreasing due to a decrease (increase) in frequency of winter (summer) MCs and an unbalanced reduction in precipitation intensity associated with intense and compact MCs that evolve under a double-jet configuration. The results highlight the individual role and potential response of each MC driver in the MHC in recent decades, and underline multiple dynamic relationships:

The growing negative contribution of summer MCs to P-E (clusters 6 and 9) reflects both their higher frequency and the rise in sea surface temperature, which enhances E over longer timescales by amplifying air-sea temperature



370 gradients (Yu 2007). The major winter clusters 1 and 4 play different roles in the MHC despite their apparent  
 371 similarity. Cluster 1 consistently provides excess P and is mostly restricted to topography, exhibiting no long-term  
 372 trend in intensity or annual P-E contributions. Cluster 4, on the other hand, travels farther from its genesis region  
 373 (mostly the lee of the Alps) and delivers excess P to the central and eastern Mediterranean, at a gradually  
 374 decreasing rate. Cluster 8, although rare, contributes substantially to P-E and shows a distinct increase in P  
 375 intensity, likely reflecting enhanced convective activity in response to rising surface temperatures – consistent  
 376 with its high convective potential (Portal et al., 2024). Finally, cluster 2 shows the steepest trend in P-E, losing  
 377 ~0.2 mm/year per affected grid-point, due to changes in mean intensity, despite a subtle rise in frequency.

378 The OHC analysis further emphasizes the independent role of each MC driver, with opposing impacts of different  
 379 MC drivers across the basin. The overall OHC loss is proportional to MC-induced E, but is generally higher due  
 380 to added sensible, radiative and advective fluxes, all of which are potentially affected by the presence of MCs. We  
 381 show that certain MCs may even add heat to the Mediterranean instead of extracting it, stressing the importance  
 382 of non-linear PV dynamics to the OHC.

383 Overall, the study reveals that each MC driver contributes differently to the MHC and OHC, with some drivers  
 384 showing opposing long-term trends. These trends are in-line with the Mediterranean precipitation paradox,  
 385 demonstrating the different dynamical responses generating it: North-Mediterranean winter MCs are indeed  
 386 showing increased precipitation rates despite their drop in frequency, while off-winter MCs frequently impacting  
 387 the southern and eastern Mediterranean are increasing in frequency and evaporation rates at the expense of  
 388 precipitation intensities, contributing to the drying of these regions.

389 The impact of MCs on the MHC agrees with the trends of total regional P derived by André et al., (2024): the “all  
 390 quartiles increase” pattern suggested for the European continent can be related to the increased P of clusters 1 and  
 391 4 often affecting the area, while the decrease in clusters 2, 6 and 9 partially explain the reduction in P intensity  
 392 across the central, eastern, and southern parts of the domain.

393 Taken together, the results show that quantifying the climate impact of MCs requires a process-based approach  
 394 that resolves their internal diversity. Each driver responds differently to warming, leading to opposing influences  
 395 on both the MHC and OHC. Long-term trends imply that the warming buffer provided by MCs is being eroded,  
 396 with severe implications for the regional hydrological budget and heat balance. Moreover, nonlinearity is expected  
 397 to strengthen in the future as shifts in both frequency and intensity align with ongoing warming for several MC  
 398 drivers.

399 The presented framework for the process-based classification and impact attribution presented here is not only  
 400 relevant for the Mediterranean but also transferable to other regions where cyclones play a critical role in  
 401 regulating hydroclimate and air-sea exchanges. Applying this methodology more broadly represents a promising  
 402 avenue for future research.

403



404 **Author contributions.** YG and SRR conceptualized the research. YG conducted the research, performed the  
405 analysis of the atmospheric data, and wrote the underlying codes and the manuscript. DKJ performed the OHC  
406 analysis and produced the corresponding figures. All coauthors took active part in reviewing and editing the  
407 final draft.

408 **Competing interests.** At least one of the (co-)authors is a member of the editorial board of Weather and Climate  
409 Dynamics. The authors have no other competing interests to declare.

410 **Acknowledgments.** This work stems from the COST Action CA19109 European network for Mediterranean  
411 cyclones in weather and climate (Hatzaki et al. 2023), supported by the European Cooperation in Science and  
412 Technology (COST; <https://www.cost.eu>, last access: 4 November 2025). We acknowledge the Israel  
413 Meteorological Service for granting access to ECMWF. The authors wish to acknowledge Enrico Scoccimaro and  
414 Dorotea Ciro Iovino of the Euro-Mediterranean Center on Climate Change (CMCC) for providing the OHC data  
415 of C-GLORIS V7, and thank them for their insightful input on an earlier version of the manuscript.

416 **Data Availability.** The composite cyclone tracks with the resulting cluster attribution are available in the  
417 supplementary assets of Givon et al., (2024a). The track labels correspond to the composite cyclone track dataset  
418 at confidence level 5, made available as a Supplement by Flaounas et al. (2023) (“TRACKS\_CL5.dat”). ERA5  
419 data are available at: [https://cds.climate.copernicus.eu/datasets/reanalysis-era5-single-](https://cds.climate.copernicus.eu/datasets/reanalysis-era5-single-levels?utm_source=chatgpt.com)  
420 [levels?utm\\_source=chatgpt.com](https://cds.climate.copernicus.eu/datasets/reanalysis-era5-single-levels?utm_source=chatgpt.com) , and details on C-GLORS v7 data availability can be found at [http://c-](http://c-glors.cmcc.it/index/index-7.html?sec=7)  
421 [glors.cmcc.it/index/index-7.html?sec=7](http://c-glors.cmcc.it/index/index-7.html?sec=7).

422 **Financial support.** This work was funded by the Israel Science Foundation (grant no. 1242/23) and the De Botton  
423 Center for Marine Science at the Weizmann Institute of Science. This work contributes to the Med-World and  
424 Tuning for Deserts Consortia, funded by the Council for Higher Education in Israel.



## 425 References

- 426 André, J., D'Andrea, F., Drobinski, P., & Muller, C.: Regimes of precipitation change over Europe and the  
 427 Mediterranean. *J. Geophys. Res. Atmos.*, 129, e2023JD040413, <https://doi.org/10.1029/2023JD040413>, 2024.
- 428 Berthou, S., Mailler, S., Drobinski, P. et al.: Lagged effects of the Mistral wind on heavy precipitation through  
 429 ocean-atmosphere coupling in the region of Valencia (Spain). *Clim Dyn.* 51, 969–983,  
 430 <https://doi.org/10.1007/s00382-016-3153-0>, 2018.
- 431 Buzzi, A., Davolio, S. & Fantini, M.: Cyclogenesis in the lee of the Alps: a review of theories. *Bull. of Atmos.*  
 432 *Sci. & Technol.* 1, 433–457, <https://doi.org/10.1007/s42865-020-00021-6>, 2020.
- 433 Cavicchia, L., H. von Storch, and S. Gualdi: Mediterranean Tropical-Like Cyclones in Present and Future Climate.  
 434 *J. Climate*, 27, 7493–7501, <https://doi.org/10.1175/JCLI-D-14-00339.1>, 2014.
- 435 Chericoni, M., Fossier, G., Flaounas, E. et al.: Unravelling drivers of the future Mediterranean precipitation  
 436 paradox during cyclones. *npj Clim. Atmos. Sci.* 8, 260, <https://doi.org/10.1038/s41612-025-01121-w>, 2025.
- 437 Flamant, C.: Alpine lee cyclogenesis influence on air-sea heat exchanges and marine atmospheric boundary layer  
 438 thermodynamics over the western Mediterranean during a Tramontane/Mistral event, *J. Geophys. Res.*, 108, 8057,  
 439 [10.1029/2001JC001040](https://doi.org/10.1029/2001JC001040), 2003.
- 440 Flaounas, E., Raveh-Rubin, S., Wernli, H. et al.: The dynamical structure of intense Mediterranean cyclones. *Clim*  
 441 *Dyn* 44, 2411–2427, <https://doi.org/10.1007/s00382-014-2330-2>, 2015.
- 442 Flaounas, E., Di Luca, A., Drobinski, P., Mailler, S., Arsouze, T., Bastin, S., Beranger K., and Lebeauupin Brossier,  
 443 C.: Cyclone contribution to the Mediterranean Sea water budget. *Clim. Dyn.* 46, 913–927,  
 444 <https://doi.org/10.1007/s00382-015-2622-1>, 2016.
- 445 Flaounas, E., Fita, L., Lagouvardos, K., and Kotroni, V.: Heavy rainfall in Mediterranean cyclones, Part II. Water  
 446 budget, precipitation efficiency and remote water sources. *Clim. Dyn.* 53, 2539–2555,  
 447 <https://doi.org/10.1007/s00382-019-04639-x>, 2019.
- 448 Flaounas, E., Davolio, S., Raveh-Rubin, S., Pantillon, F., Miglietta, M. M., Gaertner, M. A., Hatzaki, M., Homar,  
 449 V., Khodayar, S., Korres, G., Kotroni, V., Kushta, J., Reale, M., and Ricard, D.: Mediterranean cyclones: current  
 450 knowledge and open questions on dynamics, prediction, climatology and impacts, *Weather Clim. Dynam.*, 3, 173–  
 451 208, <https://doi.org/10.5194/wcd-3-173-2022>, 2022.
- 452 Flaounas, E., Aragão, L., Bernini, L., Dafis, S., Doiteau, B., Flocas, H., Gray, S. L., Karwat, A., Kouroutzoglou,  
 453 J., Lionello, P., Miglietta, M. M., Pantillon, F., Pasquero, C., Patlakas, P., Picornell, M. Á., Porcù, F., Priestley, M.  
 454 D. K., Reale, M., Roberts, M. J., Saaroni, H., Sandler, D., Scoccimarro, E., Sprenger, M., and Ziv, B.: A composite  
 455 approach to produce reference datasets for extratropical cyclone tracks: application to Mediterranean cyclones,  
 456 *Weather Clim. Dynam.*, 4, 639–661, <https://doi.org/10.5194/wcd-4-639-2023>, 2023.
- 457 Gaertner, M. A., D. Jacob, V. Gil, M. Domínguez, E. Padorno, E. Sánchez, and M. Castro: Tropical cyclones over  
 458 the Mediterranean Sea in climate change simulations, *Geophys. Res. Lett.*, 34, L14711,  
 459 <https://doi.org/10.1029/2007GL029977>, 2007.
- 460 Givon, Y., Keller Jr., D., Silverman, V., Pennel, R., Drobinski, P., and Raveh-Rubin, S.: Large-scale drivers of the  
 461 mistral wind: link to Rossby wave life cycles and seasonal variability, *Weather Clim. Dynam.*, 2, 609–630,  
 462 <https://doi.org/10.5194/wcd-2-609-2021>, 2021.
- 463 Givon, Y., Hess, O., Flaounas, E., Catto, J. L., Sprenger, M., and Raveh-Rubin, S.: Process-based classification of  
 464 Mediterranean cyclones using potential vorticity, *Weather Clim. Dynam.*, 5, 133–162,  
 465 <https://doi.org/10.5194/wcd-5-133-2024>, 2024a.
- 466 Givon, Y., Keller, D., Pennel, R., Drobinski, P. & Raveh-Rubin, S.: Decomposing the role of dry intrusions for  
 467 ocean evaporation during mistral. *Q J R Meteorol. Soc.*, 150(760), 1791–1808, <https://doi.org/10.1002/qj.4670>,  
 468 2024b.



- 469 Hatzaki, M., Flaounas, E., Davolio, S., Pantillon, F., Patlakas, P., Raveh-Rubin, S., Hochman, A., Kushta, J.,  
 470 Khodayar, S., Dafis, S., and Liberato M. L. R.: MedCyclones: Working Together toward Understanding  
 471 Mediterranean Cyclones. *Bull. Amer. Meteor. Soc.*, 104, E480–E487, [https://doi.org/10.1175/BAMS-D-22-](https://doi.org/10.1175/BAMS-D-22-0280.1)  
 472 [0280.1](https://doi.org/10.1175/BAMS-D-22-0280.1), 2023.
- 473 Hersbach H, Bell B, Berrisford P, et al.: The ERA5 global reanalysis. *Q J R Meteorol. Soc.*; 146: 1999–2049,  
 474 <https://doi.org/10.1002/qj.3803>, 2020.
- 475 Hochman, A., Alpert, P., Kunin, P. et al.: The dynamics of cyclones in the twentyfirst century: the Eastern  
 476 Mediterranean as an example. *Clim. Dyn.* 54, 561–574, <https://doi.org/10.1007/s00382-019-05017-3>, 2020.
- 477 Ilotoviz, E., Ghate, V. P., & Raveh-Rubin, S.: The impact of slantwise descending dry intrusions on the marine  
 478 boundary layer and air-sea interface over the ARM Eastern North Atlantic site. *J. Geophys. Res. Atmos.*, 126,  
 479 e2020JD033879, <https://doi.org/10.1029/2020JD033879>, 2021.
- 480 Jangir, B., Mishra, A., K., Strobach, E.: The interplay between medicanes and the Mediterranean Sea in the  
 481 presence of sea surface temperature anomalies, *Atmospheric Research* 310, 107625,  
 482 <https://doi.org/10.1016/j.atmosres.2024.107625>, 2024.
- 483 Keller Jr., D., Givon, Y., Pennel, R., Raveh-Rubin, S., and Drobinski, P.: Untangling the mistral and seasonal  
 484 atmospheric forcing driving deep convection in the Gulf of Lion: 2012–2013, *Ocean Sci.*, 18, 483–510,  
 485 <https://doi.org/10.5194/os-18-483-2022>, 2022.
- 486 Keller, D., Jr., Givon, Y., Pennel, R., Raveh-Rubin, S., and Drobinski, P.: Untangling the mistral and seasonal  
 487 atmospheric forcing driving deep convection in the Gulf of Lion: 1993– 2013. *J. of Geophys. Res. Oceans*, 129,  
 488 e2022JC019245. <https://doi.org/10.1029/2022JC019245>, 2024.
- 489 Keller Jr., D: Fractal Attractor of the Deep Convection Cycle in the Northwest Mediterranean Sea. *ESS Open*  
 490 *Archive*. [10.22541/essoar.174619871.10521682/v1](https://doi.org/10.22541/essoar.174619871.10521682/v1), 2025.
- 491 Khodayar, S., Kushta, J., Catto, J. L., Dafis, S., Davolio, S., Ferrarin, C., Flaounas, E., Groenemeijer P., Hatzaki,  
 492 M., Hochman, A., Kotroni, V., Landa, J., Láng-Ritter, I., Lazoglou, G., Liberato, M. L. R., Miglietta, M.  
 493 M., Papagiannaki, K., Patlakas, P., Stojanov, R., and Zittis, G.: Mediterranean cyclones in a changing climate: A  
 494 review on their socio-economic impacts. *Rev. Geophys.*, 63(2), e2024RG000853,  
 495 <https://doi.org/10.1029/2024RG000853>, 2025.
- 496 Klaider, N., & Raveh-Rubin, S.: Extended influence of midlatitude cyclones on global cold extremes. *Geophys.*  
 497 *Res. Lett.*, 50, e2023GL104999, <https://doi.org/10.1029/2023GL104999>, 2023.
- 498 Lebeaupin Brossier, C., Bastin, S., Béranger, K. et al.: Regional mesoscale air–sea coupling impacts and extreme  
 499 meteorological events role on the Mediterranean Sea water budget. *Clim. Dyn.* 44, 1029–1051,  
 500 <https://doi.org/10.1007/s00382-014-2252-z>, 2015.
- 501 Lionello, P. and Giorgi, F.: Winter precipitation and cyclones in the Mediterranean region: future climate scenarios  
 502 in a regional simulation. *Adv. Geosci.*, 12, 153–158, <https://doi.org/10.5194/adgeo-12-153-2007>, 2007.
- 503 Lionello, P., Boldrin, U. & Giorgi, F.: Future changes in cyclone climatology over Europe as inferred from a  
 504 regional climate simulation. *Clim. Dyn.* 30, 657–671, <https://doi.org/10.1007/s00382-007-0315-0>, 2008.
- 505 Nissen, K.M., Leckebusch, G.C., Pinto, J.G. et al.: Mediterranean cyclones and windstorms in a changing climate.  
 506 *Reg. Environ. Change* 14, 1873–1890, <https://doi.org/10.1007/s10113-012-0400-8>, 2014.
- 507 Papritz, L., S. Pfahl, H. Sodemann, and Wernli, H.: A Climatology of Cold Air Outbreaks and Their Impact on  
 508 Air–Sea Heat Fluxes in the High-Latitude South Pacific. *J. Climate*, 28, 342–364, [https://doi.org/10.1175/JCLI-](https://doi.org/10.1175/JCLI-D-14-00482.1)  
 509 [D-14-00482.1](https://doi.org/10.1175/JCLI-D-14-00482.1), 2015.
- 510 Portal, A., Raveh-Rubin, S., Catto, J. L., Givon, Y., and Martius, O.: Linking compound weather extremes to  
 511 Mediterranean cyclones, fronts, and airstreams, *Weather Clim. Dynam.*, 5, 1043–1060,  
 512 <https://doi.org/10.5194/wcd-5-1043-2024>, 2024.



- 513 Portal, A., Angelidou, A., Rousseau-Rizzi, R., Raveh-Rubin, S., Givon, Y., Catto, J.L., Battaglioli, F., Taszarek,  
 514 M., Flaounas, E. and Martius, O.: Convective Environments Within Mediterranean Cyclones. *Atmos. Sci. Lett.*,  
 515 26: e1302, <https://doi.org/10.1002/asl.1302>, 2025.
- 516 Rai, D., Raveh-Rubin, S.: Enhancement of Indian summer monsoon rainfall by cross-equatorial dry intrusions. *npj*  
 517 *Clim. Atmos. Sci.* 6, 43, <https://doi.org/10.1038/s41612-023-00374-7>, 2023.
- 518 Raveh-Rubin, S.: Dry Intrusions: Lagrangian Climatology and Dynamical Impact on the Planetary Boundary  
 519 Layer. *J. Climate*, 30, 6661–6682, <https://doi.org/10.1175/JCLI-D-16-0782.1>, 2017.
- 520 Reale, O., Feudale, L., & Turato, B.: Evaporative moisture sources during a sequence of floods in the  
 521 Mediterranean region. *Geophys. Res. Lett.*, 28(10), 2085–2088. <https://doi.org/10.1029/2000GL012379>, 2001.
- 522 Reale, M., Cabos Narvaez, W.D., Cavicchia, L. et al.: Future projections of Mediterranean cyclone characteristics  
 523 using the Med-CORDEX ensemble of coupled regional climate system models. *Clim. Dyn.* 58, 2501–2524,  
 524 <https://doi.org/10.1007/s00382-021-06018-x>, 2022.
- 525 Rieder, J. C., Aemisegger, F., Dente, E., and Armon, M.: Meteorological ingredients of heavy precipitation and  
 526 subsequent lake-filling episodes in the northwestern Sahara, *Hydrol. Earth Syst. Sci.*, 29, 1395–1427,  
 527 <https://doi.org/10.5194/hess-29-1395-2025>, 2025.
- 528 Rousseau-Rizzi, R., Raveh-Rubin, S., Catto, J. L., Portal, A., Givon, Y., and Martius, O.: A storm-relative  
 529 climatology of compound hazards in Mediterranean cyclones, *Weather Clim. Dynam.*, 5, 1079–1101,  
 530 <https://doi.org/10.5194/wcd-5-1079-2024>, 2024.
- 531 Saaroni, H., Halfon, N., Ziv, B., Alpert, P. and Kutiel, H.: Links between the rainfall regime in Israel and location  
 532 and intensity of Cyprus lows. *Int. J. Climatol.*, 30: 1014–1025, <https://doi.org/10.1002/joc.1912>, 2010.
- 533 Scoccimarro, E., Borrelli, A., Sangelantoni, L., Cavicchia, L., Tibaldi, S., & Boccaletti, G.: A cul-de-sac effect  
 534 makes Emilia-Romagna more prone to floods in a changing climate. *Sci Rep* 15, 36823.  
 535 <https://doi.org/10.1038/s41598-025-24486-7>, 2025.
- 536 Simón Ruiz, Damià Gomis, Marcos G. Sotillo, Simon A. Josey: Characterization of surface heat fluxes in the  
 537 Mediterranean Sea from a 44-year high-resolution atmospheric data set, *Global and Planetary Change*, 63(2–3),  
 538 258–274, <https://doi.org/10.1016/j.gloplacha.2007.12.002>, 2008.
- 539 Stathopoulos, C., Patlakas, P., Tsalis, C., & Kallos, G.: The Role of Sea Surface Temperature Forcing in the Life-  
 540 Cycle of Mediterranean Cyclones. *Remote Sensing*, 12(5), 825, <https://doi.org/10.3390/rs12050825>, 2020.
- 541 Storto, A. and Masina, S.: C-GLORSv5: an improved multipurpose global ocean eddy-permitting physical  
 542 reanalysis, *Earth Syst. Sci. Data*, 8, 679–696, <https://doi.org/10.5194/essd-8-679-2016>, 2016.
- 543 Strobach, E., Mishra, A.K., Jangir, B. et al.: Intensification of a rain system imparted by Mediterranean mesoscale  
 544 eddies. *Sci. Rep.* 14, 26810, <https://doi.org/10.1038/s41598-024-76767-2>, 2024.
- 545 Thurnherr, I., Hartmuth, K., Jansing, L., Gehring, J., Boettcher, M., Gorodetskaya, I., Werner, M., Wernli, H., and  
 546 Aemisegger, F.: The role of air–sea fluxes for the water vapour isotope signals in the cold and warm sectors of  
 547 extratropical cyclones over the Southern Ocean, *Weather Clim. Dynam.*, 2, 331–357, <https://doi.org/10.5194/wcd-2-331-2021>, 2021.
- 549 Tootoonchi, R., Bordoni, S., and D'Agostino, R.: Revisiting the moisture budget of the Mediterranean region in  
 550 the ERA5 reanalysis, *Weather Clim. Dynam.*, 6, 245–263, <https://doi.org/10.5194/wcd-6-245-2025>, 2025.
- 551 Yu, L.: Global Variations in Oceanic Evaporation (1958–2005): The Role of the Changing Wind Speed. *J.*  
 552 *Climate*, 20, 5376–5390, <https://doi.org/10.1175/2007JCLI1714.1>, 2007.
- 553 Zappa, G., Hawcroft, M.K., Shaffrey, L. et al.: Extratropical cyclones and the projected decline of winter  
 554 Mediterranean precipitation in the CMIP5 models. *Clim. Dyn.* 45, 1727–1738, <https://doi.org/10.1007/s00382-014-2426-8>, 2015.



- 556 Zittis, G., Hadjinicolaou, P., Klangidou, M. et al.: A multi-model, multi-scenario, and multi-domain analysis of  
557 regional climate projections for the Mediterranean. *Reg. Environ. Change* 19, 2621–2635,  
558 <https://doi.org/10.1007/s10113-019-01565-w>, 2019.
- 559 Zittis, G., Almazroui, M., Alpert, P., Ciais, P., Cramer, W., Dahdal, Y., et al.: Climate change and weather  
560 extremes in the Eastern Mediterranean and Middle East. *Reviews of Geophysics*, 60,  
561 e2021RG000762, <https://doi.org/10.1029/2021RG000762>, 2022.